New Materials for 193-nm Trilayer Imaging

Jim D. Meador[a], Doug Holmes[a], Mariya Nagatkina[a], Rama Puligadda[a],
Denise Gum[a], Randy Bennett[a], Sam Sun[a], Tomoyuki Enomoto[b]
[a]Brewer Science, Inc., 2401 Brewer Drive, Rolla, MO65401
[b]Toyama R&D Center, Nissan Chemical Industries, LTD., 635 Sasakura, Fuchu-Machi, Neigun,
Toyama, 939-2792, Japan

ABSTRACT

This paper presents our progress in developing spin-on, thermosetting hardmasks and bottom antireflective coatings (BARCs) for 193-nm trilayer usage. Binder materials that were used in preparing the silicon-containing hardmasks include polymers with pendant alkyl silane function and various polyhedral oligomeric silsesquioxane (POSS) substances, with the hardmasks being very transparent at both 193 and 248-nm. The second generation hardmasks offer significant improvements over earlier materials[1] in O_2 plasma etching resistance. The etching selectivity (O_2 plasma) for the best-case hardmask to a trilayer BARC is about 31.5 (15 sec etch), with the selectivity number being much higher for longer etching times. The preferred hardmask is both spin-bowl and solution compatible. The new trilayer BARCs use low molecular weight binders that are rich in aromatic content for halogen plasma etching resistance, but the antireflective products also feature optical parameters that allow $\leq 0.4\%$ reflectivity into the photoresist on a silicon substrate. At about 500-nm film thickness, selected BARCs have provided 80-95% planarity over 2,000Å topography. Combining the two thermosetting products (hardmask and BARC) with a thin 193-nm photoresist in a trilayer configuration has given excellent 80-nm L/S (1:1) after exposure and wet-development. A conventional resist has provided 100-nm L/S (1:1.4).

Keywords: 193-nm microlithography, 248-nm, trilayer, spin-on, hardmask, antireflective, BARC

1. INTRODUCTION

The prime function of the photoresist in trilayer usage is simply imaging and not masking. This differs from both single layer and bilayer processing were the resist performs both functions. Trilayer processing thus offers the opportunity for a significant reduction in photoresist film thickness and provides a potential solution to the familiar aspect ratio problem encountered during wet development of 193-nm single layer resists. Trilayer systems are unique in allowing optimum thickness control for the imaging, masking, and antireflective layers. An additional advantage for trilayer compared to bilayer processing includes using conventional or preferably ultra-thin resists rather than the developmental silicon-containing bilayer materials. Per our design,[1] the trilayer stack consists of the following: 1) a conventional or preferably ultra-thin 193-nm resist as the top layer, 2) an oxygen plasma-resistant hardmask which separates the photoresist and BARC and serves as the mask during transfer of the pattern to the BARC, and 3) a BARC which is designed to provide thick, planarizing films and be resistant to a halogen plasma and serve as the mask during transfer of the pattern to the substrate. As a benefit resulting from the thick and highly etch resistant BARC mask, the trilayer processing scheme offers the potential for transferring the resist pattern to great depths into the substrate. In order to optimize trilayer processing new 193-nm materials (hardmasks and BARCs) will be required to meet demanding imaging, etching, and processing specifications. As an example of the exacting requirements for these materials, a very large O_2 etching selectivity between the BARC and hardmask is not by itself a sufficient etching specification for these materials. Both products must meet other demanding etching resistance requirements to adequately fulfill their respective roles as masks. This paper describess the chemistry and properties of the two types of trilayer products, with both hardmask and BARC being spin-on and thermosetting. There has presently been no effort to measure silicon outgassing during 193-nm exposures, with an expectation that the covering photoresist will minimize or eliminate this problem.[2] The plasma etching gases (CF_4 and O_2) that were used throughout the study are first generation efforts and may not provide optimum performance.

2. METHODOLOGY

Safe-solvents such as propylene glycol monomethyl ether acetate (PGMEA), propylene glycol monomethyl ether (PGME), propylene glycol monopropyl ether (PnP), ethyl lactate (EL) or combinations of same were used in formulating all described spin-on hardmasks and BARCs. While the spin application parameters varied, thermal cure was always at 205°C for 60 sec with the hotplate under vacuum. A Tencor Alpha-Step 200 and/or a Gaertner ellipsometer were used to measure film thickness of the cured coatings on a silicon substrate. Absorbance of the cured films at 193-nm was measured on a quartz substrate using a Cary 500 Scan UV-Vis-NIR spectrophotometer, with the ODs then calculated from the absorbance and thickness data. The standard EL stripping test was used to assess insolubility of the thermally cured coatings.[3,4] The procedures for the spin-bowl and solution compatibility tests have been described in earlier publications.[1,5,6] The real (n) and imaginary (k) parts of the refractive index for a product were determined using a Variable Angle Spectroscopic Ellipsometer (VASE®) instrument from J. A. Woollam. The 193-nm exposures of trilayer stacks and subsequent wet-development procedures were carried out at IMEC. The scanning electron microscope (SEM) photos of cross-sectioned wafers were prepared at Brewer Science or IMEC. Plasma etching rates, using either CF_4 or O_2 as the gas, were measured using a Trion etcher. The selectivities were then calculated from the etching rates. The measurements of BARC planarity on topography wafers were made by Brewer Science's SEM department using photos of cross-sections. For the calculation of percent planarity, the % conformality is subtracted from 100%.[5]

3. RESULTS AND DISCUSSION

3.1 Spin-on hardmasks for trilayer usage

The hardmask coatings are comprised of a crosslinkable binder material, an aminoplast(s), solvent(s), and catalyst(s). The binders, which are silicon-containing, were from two different chemistry platforms: a) polymers with pendant alkyl silane function and b) POSS-containing materials. The former type of product (first generation) was highlighted in a previous publication and will receive limited attention in this paper.[1] The first generation family of hardmasks offered many good properties, but the products suffered from mediocre O_2 plasma etching resistance due to low silicon content and the best-case products were marginally spin-bowl compatible. Our best-case first generation hardmask, cited herein as a reference material, was product A. This product gave very dependable coat quality. The best-case POSS-type hardmask α, (highlighted in this paper) is far superior to first generation product A in O_2 plasma etching resistance, spin-bowl compatibility, and also in imageability. Of importance, the O_2 plasma etching rates of the silicon-containing hardmasks are not linear with etching times. As the concentration of silicon oxide(s) builds during the etching process with etching time, the hardmask etching rate slows. This is shown for hardmask A in Figure 1. During the first 50 sec of the etch about 52-nm of hardmask film is removed, while in the next 50 sec only about 18-nm of coating is etched away. The high initial O_2 plasma etching rate raises some concerns about etch bias problems for hardmask A during the BARC open step and suggests a need for higher silicon-content and slower etching hardmasks. Using a CF_4 plasma, the etching rates of the silicon-containing hardmasks do not vary with etching times.

3.1.1   First generation alkyl silane hardmasks (thick films)

Hardmask A was very dependable for trouble-free coat quality, but somewhat suspect in O_2 plasma etching resistance. The silicon content of this product's binder polymer was 11.1%, while the silicon content of the dried hardmask film was 8.6%. An approach to improving the masking capabilities of the hardmask in an O_2 plasma during the open of thick BARC films was to simply increase film thickness. This was easily done by increasing the solids in the coating from the standard 3.3 to 6.0%, keeping the ratios of all constituents other than solids to solvent constant. A spin application of the new hardmask B at 1550 rpm, followed by thermal cure gave a 211-nm thick film. A trilayer stack comprised of Arch Chemicals ultra-thin resist GARS8207K21 (150-nm)/hardmask B (211-nm)/BARC 1 (481-nm) gave good 80-nm L/S (1:1.4) after wet-development. The SEM photos, showing 0.7 μm DOF are shown in Figure 2. While the lithography was good using the thick hardmask approach, applications may[2] be limited due to the etch bias concerns during the plasma etch steps.
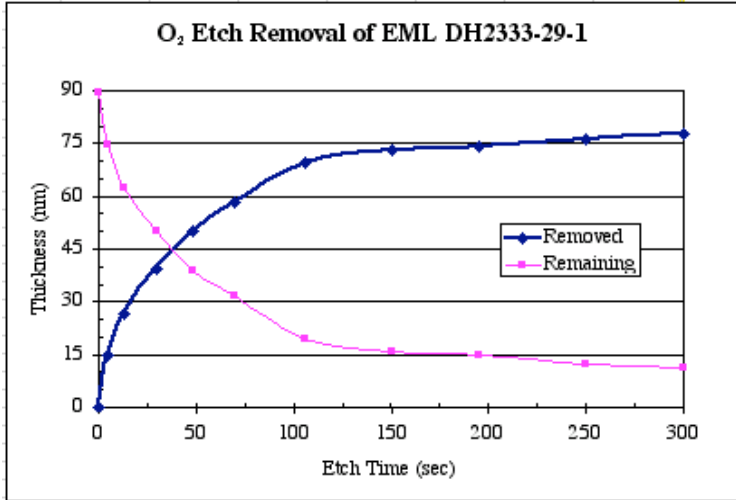
Figure 1. Non-linear etch rate of first generation hardmask A with an O_2 plasma.

Arch Chemicals resist GARS8207K21 on hardmask B on BARC 1 (150-nm/211-nm/481-nm; 80-nm L/S (1:1.4); 0.7 μm DOF.
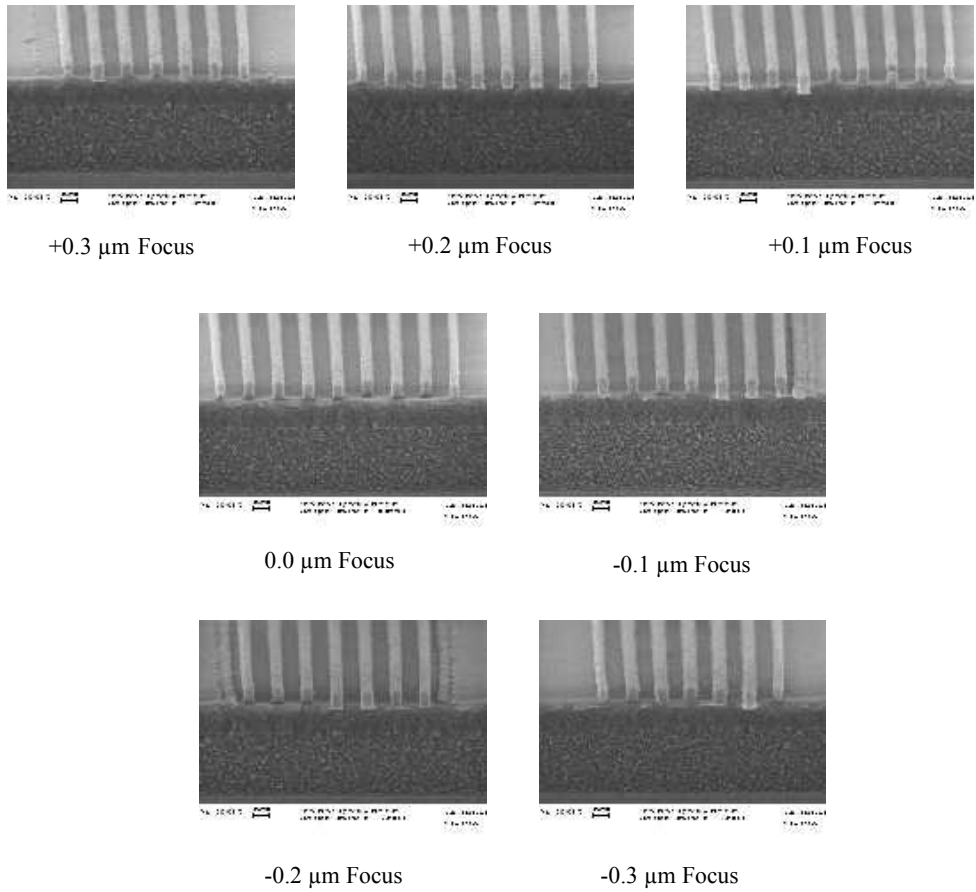

+0.3 μm Focus

+0.2 μm Focus

+0.1 μm Focus

0.0 μm Focus

-0.1 μm Focus

-0.2 μm Focus

-0.3 μm Focus

Figure 2. Trilayer imaging using th   tion hardma

3.1.2   Second generation POSS-type hardmasks

Numerous aminoplast-crosslinkable POSS binders were screened for applicability in preparing spin-on hardmasks. The solvent(s) for these products was either PGMEA or PGMEA/PGME. Selected data is shown in Table 1 for four different POSS binders and seven different hardmask formulations. Incorporating a binder into different aminoplast formulations may give radically differing properties. Silicon content in the dried POSS-type hardmask films varied from 12 to 22%. For second generation α, the percent silicon percentage in the dried film was 156% greater than for first generation product A. The silicon contents are calculated values and not measured numbers. A problem that was sometimes observed in applying the POSS hardmasks directly onto silicon wafers was small coating defects (pinpoints, voids, etc.) in the cured film. Hardmask α (the preferred second generation product) does not give this problem on re-polished wafers nor was it observed on application to trilayer BARC 2. Hardmask α was evaluated at either 3 or 5% solids levels during this study, with the ratios of all constituents other than solvent to solids held constant. Depending on the formulation and POSS binder, adhesion of the photoresist during exposure and wet-development was also sometimes a problem. Hardmask ε exhibited this problem. These are deficiencies (cured film defects and adhesion) that were never observed with the very process friendly alkyl silane-type products. The film thicknesses shown in Table 1 were measured with an ellipsometer and used in calculating OD. Film thicknesses can obviously be changed by varying spin application and cure conditions or the percent solids in the hardmask coating. The POSS-type hardmasks, as designed, are relatively optically transparent at 193-nm as shown by the ODs and VASE-measured optical parameters. Dividing the spectrophotometer-measured 193-nm OD by 28.28 gives a calculated k-value, which in these examples agree well with the VASE data for same constant.[6] The shown POSS-type hardmasks are also very transparent at 248-nm and may find applications at that wavelength. The thermoset hardmask coatings were well insolubilized during the hotplate bake step as indicated by the absence of thickness loss during the EL stripping tests.

Table 1. POSS-type hardmask silicon content, and 193-nm cured film properties.

Identity of Hardmask	Weight % Silicon in Hardmask Solids	POSS Binder	Film Thickness, nm	OD at 193-nm	193-nm k-value Calculated from OD	193-nm Optical Parameters (VASE) n k	248-nm Optical Parameters (VASE) n k	EL Stripping
α*	22.0	I	61.0	2.51	0.09	1.67 0.064	1.57 0.000	-0.07%
β	20.2	I	65.8	1.96	0.07	1.68 0.067	1.56 0.014	+0.09%
χ	15.0	II	88.5	0.95	0.03	1.65 0.025	1.56 0.002	+0.85%
δ	13.2	II	73.6	1.60	0.06	1.66 0.059	- -	+0.43%
ε	13.2	III	114.8	0.65	0.02	1.65 0.016	1.56 0.001	+0.28%
φ	11.9	III	90.7	1.19	0.04	1.66 0.036	1.56 0.01	+0.44%
γ	11.9	IV	120.2	0.54	0.02	1.67 0.026	1.57 0.002	+0.57%

*preferred POSS-containing hardmask

3.1.2.1   Spin-bowl Compatibility of POSS-type hardmasks

The solids from a spin-on hardmask or BARC should readily re-dissolve in solvent(s) at ambient conditions to minimize build-up on the walls of the spin-bowl. A passing value for this property (spin-bowl compatibility) by our test procedure is considered to be ≥ 90% re-solubility. The best of the POSS-type hardmasks exhibit this re-dissolution performance, which may be related to the binder chemistry and/or the formulation constituents. Table 2 gives the composite re-dissolution data for six solvents: acetone, cyclohexanone, 2-heptanone, PGME, EL, and PGMEA. The products α and χ are very re-dissolvable (i.e., spin-bowl compatible) in solvents, while using the same binders in different formulations (β and δ) resulted in unacceptable re-dissolution.

Table 2. Spin-bowl compatibility data for POSS-type hardmasks.

Identity of Hardmask	POSS Binder	Composite Spin-bowl Compatibility
α*	I	98.0%
β	I	10.2%
χ	II	96.7%
δ	II	70-75%
ε	III	94.2%

*preferred POSS-containing hardmask

3.1.2.2 Solution Compatibility of POSS-type hardmasks

To be certain that there will be no precipitation of the hardmask solids in the drain lines or spin-bowl, the coating is expected to be very compatible to mixing with solvents and photoresists. The best-case hardmask α (at 5% solids) was tested for solution compatibility by mixing 1.0 g of the hardmask solution with 9.0 g of solvent/photoresist and then 9.0 g of hardmask coating with 1.0 g of resist at ambient conditions. The following solvents/resists gave no failures: PGME, cyclohexanone, EL, PnP, 2-heptanone, ∂-butyrolactone, acetone, and deep-UV photoresist APEX-E.

3.1.2.3 Plasma etching selectivities of POSS-type hardmasks to first generation product A

The etching selectivity data for POSS-type hardmasks to the first generation product A is shown in Table 3 for a range of etching times, with the O_2 plasma etching rates for the hardmasks being non-linear with etching time. Not surprisingly, the highest silicon-content hardmask α gives the slowest etch rates. The etching rate for this product is about 1/4 that of first generation A. The slow O_2 plasma etching hardmask will allow the use of very thin hardmask films (desired) and additionally minimize any etch bias concerns for the middle layer during the BARC open step. As opposed to an O_2 plasma, etching product α in a CF_4 plasma resulted in an ~ 10% increase in etch rate relative to first generation hardmask A. The etching selectivity of α to Arch Chemical's photoresist GAR8105G1 with the fluorinated gas was about 1.83. Thus, this POSS-type hardmask will open quickly during the CF_4 etch step minimizing the loss of photoresist.

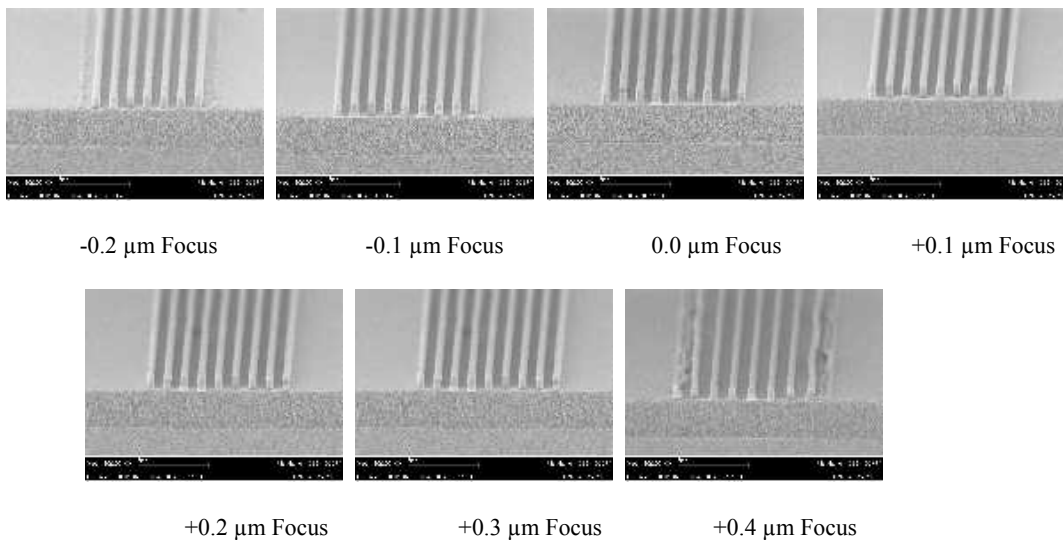Table 3. O_2 and CF_4 plasma etching selectivities of POSS-type hardmasks to product A.

Identity of EML	Etching Gas	Etching Selectivity to Hardmask A	Etching Times, seconds
α*	O_2	0.21-0.27	15-60
β	O_2	0.30-0.32	20-50
δ	O_2	0.37-0.41	15-45
α*	CF_4	1.06-1.07	10-30
β	CF_4	1.65-1.70	10-15
δ	CF_4	1.06	15-23

*preferred POSS hardmask

3.1.2.4 Trilayer lithography using a POSS-type hardmask and a trilayer BARC

The trilayer stacks consisted of a 193-nm photoresist on top of a thermoset hardmask on top of a thermoset BARC. Using Arch Chemicals 193-nm thin resist GARS8107A10 (200-nm film thickness), excellent 80-nm L/S (1:1) were achieved with hardmask α and trilayer BARC 2. The depth-of-focus (DOF) was at least 0.6 µm. The spaces between the lines appeared to be relatively clean. Using JSR's conventional 193-nm photoresist AR237J (230-nm film thickness) with the same hardmask and BARC combination gave clean 100-nm L/S (1:1.4), with about 0.7 µm DOF. The SEM photos for both trilayer stacks may be seen in Figure 3. These examples represent some of the better wet-developed images obtained from trilayer processing. The hardmask α has been selected for additional optimization studies based on the following: a) solution and spin-bowl compatibility, b) outstanding etching properties, and c) excellent lithography.

a) JSR resist AR237J on hardmask α on BARC 2 (230-nm/63.4-nm/480.4-nm respectively); 100-nm L/S (1:1.4); 0.7 μm DOF

| -0.2 μm Focus | -0.1 μm Focus | 0.0 μm Focus | +0.1 μm Focus |

| +0.2 μm Focus | +0.3 μm Focus | +0.4 μm Focus |

b) Arch Chemicals GARS8107A10 on hardmask α on BARC 2 (200-nm/63.4-nm/480.4-nm respectively); 80-nm L/S (1:1); 0.6 μm DOF

| -0.3 μm Focus | -0.2 μm Focus | -0.1 μm Focus | 0.0 μm Focus |

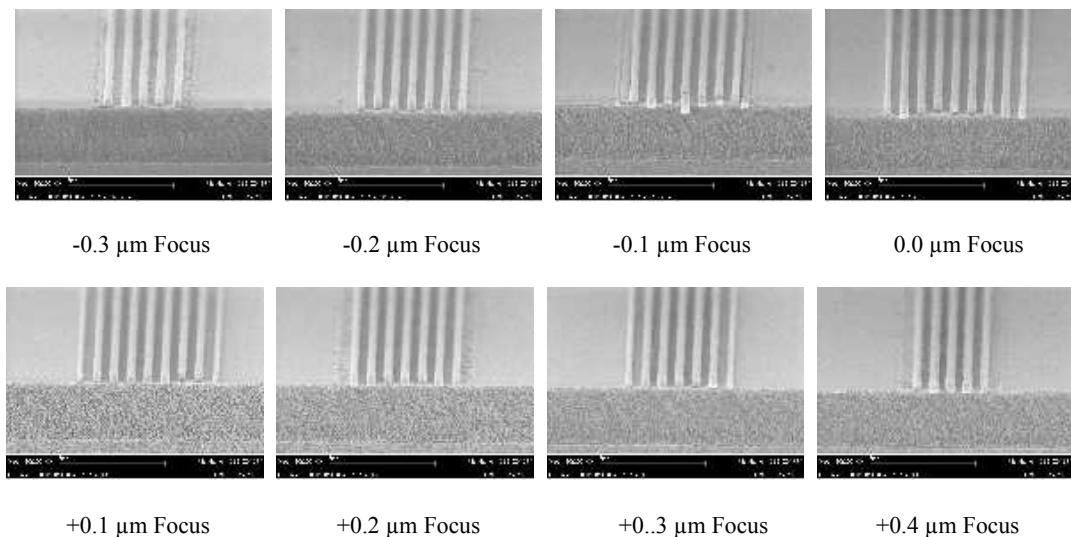| +0.1 μm Focus | +0.2 μm Focus | +0..3 μm Focus | +0.4 μm Focus |

Figure 3. Trilayer imaging using a JSR and an Arch Chemicals 193-nm photoresist

3.2   193-nm trilayer BARCs

The functions of the BARC in trilayer processing include: a) reflection control during exposure of the photoresist, b) planarizing the substrate prior to application of the hardmask and resist, and c) masking during transfer of the pattern to the substrate. A trilayer BARC must exhibit numerous properties to fulfill these roles including appropriate optical parameters, excellent planarizing performance, a high O_2 plasma etching selectivity to the hardmask during the BARC open step, and outstanding resistance to the halogen plasma used in transferring the pattern to the substrate. The BARC must also be processing friendly, exhibiting trouble-free thick film coat quality and solution and spin-bowl compatibility. In trilayer usage, chemical interactions between the photoresist and BARC should be minimal due to the separating hardmask. This allows added latitude in the BARC's formulation, as compared to single layer and bilayer applications. The properties of five second generation multilayer BARCs are highlighted, with three of these products provided by Nissan Chemical. All presented properties data was measured by Brewer Science. The binder polymers for these products are low molecular weight materials to enhance planarity over topography.

3.2.1   Properties of second generation trilayer BARCs

The performance of the five BARCs is shown in Table 4. The solvent(s) for products 1 and 2 is PnP, while the three other products use EL/PGME. The former product (1) was our standard for many months, but the other four BARCs provide superior CF_4 plasma etching resistance. As may be seen, all products show an outstanding blend of processing and optical properties. Coat quality for BARC 4 was still excellent at 501-nm film thickness. The 193-nm optical parameter data was measured with a VASE. The k-values are low consistent with excellent reflectance control using thick BARC films, but the products also exhibit excellent resistance to a CF_4 plasma as expected from high aromatic content BARCs. The k-values calculated from the ODs agree relatively well with the VASE data. There were no significant thickness losses during the EL stripping tests indicating acceptable thermal cures. The film thickness for product 2 was stable for > 3 months, increasing by only +0.70% using identical spin/cure conditions; however, a faint striation problem was observed in the aged film suggesting a potential need for optimizing the solvent system. Applying about 515-nm of BARC 1 onto a 200-nm topography wafer resulted in 84-95% planarity over 1/1, 1/2, and 1/4 L/S for 0.35 µm features. Using 490-nm of product 2 on a 200-nm topography wafer the values were 80-94% planarity over 1/1, 1/2, and 1/4 L/S for 0.35 µm features. The two thickness measurements for the planarity study were made with the Alpha-Step 200.

Table 4. Performance of trilayer BARCs.

Identity of BARC	Film Thickness	OD at 193-nm	193-nm k-value Calculated from OD	Initial Coating Quality	EL Stripping	193-nm Optical Parameters (VASE)		% Planarity, 200-nm Topography
						n	k	
1	426.1-nm	6.04	0.21	good	0.00%	1.78	0.202	84-95
2	480.4-nm	5.37	0.19	good	+0.04-+0.16%	1.68	0.167	80-94
3	257.0-nm	8.32	0.29	good	+0.24	1.60	0.28	-
4	273.5-nm	9.20	0.33	good	-0.05	1.56	0.28	-
5	305.6-nm	8.57	0.30	good	-0.09	-	-	-

3.2.1.1   Spin-bowl Compatibility of BARCs

The BARCs are extremely spin-bowl compatible. The composite spin-bowl compatibility data for product 1 differs from the norm (see sub-section 3.1.1.1) in that only five solvents were tested, with cyclohexanone being the eliminated solvent. The spin-bowl compatibility test for BARC 2 was also with only five solvents, with 2-heptanone now being the missing solvent. For the other three BARC, the standard six solvents were used in the testing, but with cyclopentanone replacing cyclohexanone. The data is shown in Table 5.

Ttable 5. Spin-bowl compatibility of trilayer BARCs.

Identity of BARC	Composite Spin-bowl Compatibility
1	99.5
2	98.6
3	99.3
4	99.4
5	98.0

3.2.1.2 Plasma Etching Rates of New Trilayer BARCs

The etching selectivity of BARC 1 to second generation hardmask α with O_2 was 31.5 for a 15 sec etch. Using the same gas composition, the etching selectivity for BARC 1 to first generation hardmask A was 11.5 for a 60 sec etch. While BARC 1 features a very attractive balance of properties, tests in the field brought a request for improved etching resistance to a halogen plasma. To quantify the extent of improvement in etching resistance for the four other products compared to BARC 1, the BARCs were all etched using the Trion etcher with CF_4 as gas. The percentage reduction in etching rate was in the 20-25% range for the products 3, 4, and 5 and 12-17% for product 2 relative to BARC 1. Based on the presented properties, these are all promising BARCs. The etch data is shown in graphical form in Figure 4.
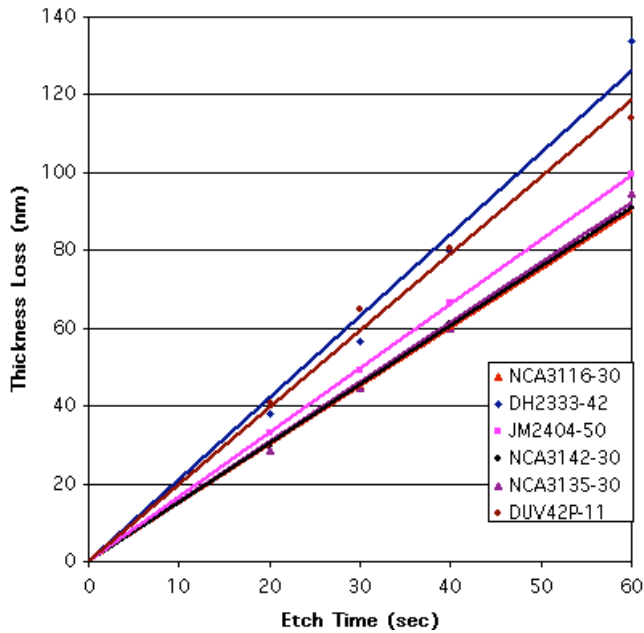

Figure 4. CF_4 plasma etching rate curves for trilayer BARCs using the Trion etcher.

3.2.1.3 Prolith modeling

Prolith/2 version 7.2.0 was used to model acceptable n and k-values for a 500-nm thick BARC film that is under 60-nm of hardmask α and 330–nm of photoresist AR237J. As shown in the Figure 5 graph, to achieve 0.2-0.4% reflectivity into the photoresist, a k-value of ≤ 0.29 is acceptable for n-values between 1.55 and 1.9. The VASE-measured optical parameters of all five BARCs highlighted in this paper are within these ranges. For BARC k-values that are greater than 0.36, there is no n-value that will give a comparably low reflectivity. Lowering the BARC k-value to 0.17, the value measured for product 2, will give $\leq 0.20\%$ reflectivity into the resist for n-values in the range of 1.55 to 1.9.
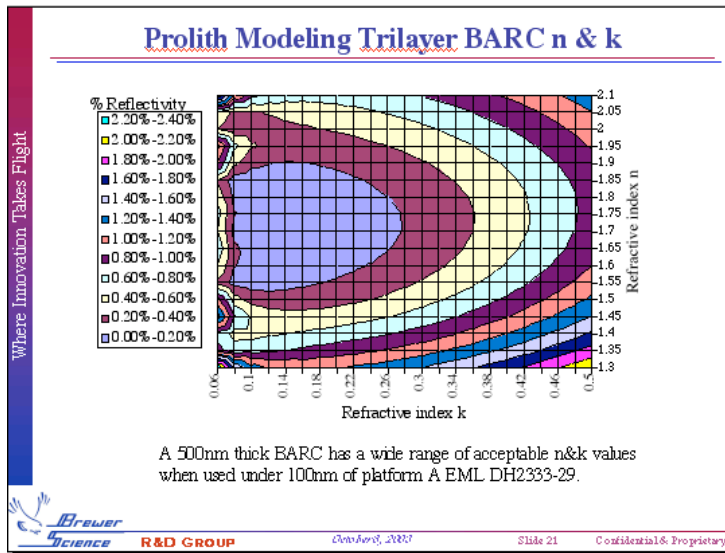
Figure 5   Percent reflectivity into the photoresist versus trilayer BARC n and k values.

4. CONCLUSIONS

This paper described our progress in designing second generation spin-on hardmasks and BARCs for use in 193-nm trilayer imaging. Hardmasks (silicon-containing) were prepared that gave outstanding 80-nm L/S (1:1) when used in a trilayer imaging stack, O_2 etching rates that were 1/4 those of first generation hardmasks, and spin-bowl and solution compatibility. Etching selectivity of a trilayer BARC to this hardmask in an O_2 plasma was about 31.5. New 193-nm BARCs were prepared for trilayer applications that exhibit: a) outstanding etching resistance in a CF_4 plasma, b) optical parameters that assure low reflectivity into the photoresist, and c) desirable processing performance. Several of the new BARCs plasma etch 20-25% slower using CF_4 than the previous standard. Our future efforts on the trilayer scheme will be aimed at plasma transferring the resist pattern to the hardmask, to the BARC, and to the substrate.

ACKNOWLEDGMENTS

REFERENCES

1. Jim D. Meador et al., "193-nm Multilayer Imaging Systems," Proc. SPIE, **5039**, p. 948, 2003.
2. M. Slezak, "Multilayer resist strategies," Solid State Technology, July 2003, p. 38.
3. G. Xu et al., "New Antireflective Coatings for 193 nm Lithography," Proc. SPIE, **3333**, p. 524, 1998.
4. Jim D. Meador et al., "Recent Progress in 193 nm Antireflective Coatings," Proc. SPIE, **3678**, p. 800,1999.
5. J. Meador et al., "Second-Generation 193-nm Bottom Antireflective Coatings (BARCs)," Proc. SPIE, **3999**, p.1009, 2000.
6. J. Meador et al., "Improved Crosslinkable Polymeric Binders for 193-nm Bottom Antireflective Coatings (BARCs)," Proc. SPIE, **4345**, p.846, 2001.